Progress In Electromagnetics Research C, Vol. 171, 447–457, 2026 PIER C

(Received 13 March 2026, Accepted 22 April 2026, Scheduled 8 July 2026)

Optimized Circularly Polarized Truncated Square Patch Antenna for Satellite Communications Using Genetic Algorithm

Abdelilah Ait Lahcen[1], Lahcen Sellak[2], Asma Khabba[3], Samira Chabaa[4], Saïda Ibnyaich[1], Abdelouhab Zeroual[1], Zahriladha Zakaria[5]*, Abdullahi Yahye Ahmed[6], and Ahmed Jamal Abdullah Al-Gburi[7]*

[1]*LISI Laboratory, Faculty of Science Semlalia, UCA, Cadi Ayyad University I2SP Team, Bd. Prince My Abdellah, Marrakech, Morocco*
[2]*Electrical Engineering Department, LCCPS Laboratory, Higher National School of Arts and Crafts UH2C, Hassan II University, Casablanca, Morocco*
[3]*LAMIGEP Laboratory, Morrocan School of Engineering Sciences (EMSI), Marrakesh, Morocco*
[4]*Industrial Engineering Department, LISAD Research Laboratory, National School of Applied Sciences UIZ, Ibn Zohr University, Agadir, Morocco*
[5]*Center for Telecommunication Research & Innovation (CeTRI) Fakulti Teknologi Dan Kejuruteraan Elektronik Dan Komputer (FTKEK), Universiti Teknikal Malaysia Melaka (UTeM) Jalan Hang Tuah Jaya, 76100, Durian Tunggal, Melaka, Malaysia*
[6]*SIMAD University, Jidka Warshadaha 2526, Mogadishu, Somalia*
[7]*Strategic Research Institute (SRI), Asia Pacific University, Jalan Teknologi 5 Taman Teknologi Malaysia, 57000, Kuala Lumpur, Malaysia*

ABSTRACT: Manually optimizing the performance of a circularly polarized (CP) patch antenna typically requires numerous iterative adjustments and can be highly time-consuming. To address this challenge, artificial intelligence techniques can be employed to efficiently explore the parameter and solution spaces. In this work, a well-known genetic algorithm (GA) is utilized to design and optimize a novel CP antenna. Specifically, a multi-objective genetic algorithm (MOGA) is adopted as a powerful optimization tool, providing effective exploration of the parameter space to achieve the desired operating bandwidth and CP characteristics. The optimized CP antenna features a compact size of 20 mm $\times$ 20 mm $\times$ 1.6 mm. The design process is carried out using HFSS and MATLAB, and the results are further validated through simulations in CST and ADS (equivalent circuit modeling). The antenna is fabricated by etching the patch and ground plane on the top and bottom sides of an FR-4 epoxy substrate ($\varepsilon_r = 4.4$), respectively. The simulated reflection coefficient bandwidth (RCBW) and axial ratio bandwidth (ARBW) are significantly enhanced, achieving fractional bandwidths of 25.78% and 16.68%, respectively, while the measured RCBW reaches 24.5%. Furthermore, the proposed antenna provides a peak gain of 5.9 dBi and a radiation efficiency exceeding 67%. The application of MOGA effectively enhances both the operating bandwidth and CP performance, making the proposed antenna a strong candidate for various Ku-band applications.

1. INTRODUCTION

CP patch antennas are an essential class of radiating elements in modern wireless systems because of their inherent benefits in maintaining high signal reliability [1], reducing interference [2], and suitability for mobile applications [3]. Circularly polarized antennas are widely used in several applications, namely satellite [4, 5], maritime radar communications [6], and wireless communication systems. Regardless of the orientation between the transmitting and receiving ends, CP antennas, in contrast to linearly polarized antennas, consistently maintain signal integrity [7]. This type of microstrip antenna is developed to transmit and receive electromagnetic waves with CP, meaning that the electric field propagates in a circular direction as the wave progresses. CP is achieved by exciting two orthogonal modes of the patch antenna with equal magnitude and difference phase of 90 degrees [8]. Numerous design mechanisms exist, such as truncated square [9] or circular patch [10], adding perturbation elements [11], utilizing dual feedlines with a phase difference of 90 degrees [12]. The optimization of the CP antenna performance can be performed using manual trial-and-error method, which demands several iterations and more time to achieve the desired characteristics. To handle these challenges, different artificial intelligence techniques may be implemented, including Particle Swarm Optimization (PSO) [13], Ant Colony Optimization (ACO) [14], MOGA [15], and artificial neural network (ANN) [16, 17].

Numerous studies have been performed in the literature, such as in [18]. The proposed antenna is designed to create CP by feeding two orthogonal modes, which are achieved by using a 90-degree power divider. To improve the gain, two tech-

* Corresponding authors: Ahmed Jamal Abdullah Al-Gburi (ahmedjamal@ieee.org); Zahriladha Zakaria (zahriladha@utem.edu.my).

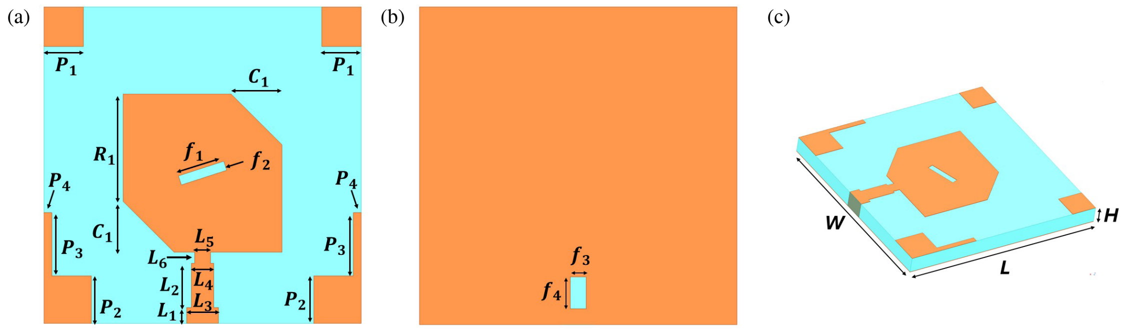

FIGURE 1. Optimized antenna structure and its parameters, (a) front side, (b) back side, and (c) 3D view.

niques are used, including 9×9 rectangular unit cells and a solid sheet of copper. This antenna operates within the bandwidth (BW), ranging from 10 to 13.54 GHz. Moreover, it is CP in the frequency band from 10.5 to 12.5 GHz. Also, it offers a maximum gain close to 8.5 dBi. Furthermore, paper [19] presents a circular patch antenna with a rectangular slot utilized to generate CP. In order to broaden the band of CP radiation, a 6×6 array of slotted circular metasurface (MTS) unit cells is used. This MTS CP antenna is designed on an FR4 ($\varepsilon_r = 4.3$) substrate, providing an entire size of 38.7 mm $\times$ 38.7 mm $\times$ 3.4 mm. It operates in the band from 5.18 to 7.4 GHz. The CP bandwidth ranges from 5.48 to 7.05 GHz. Furthermore, paper [20] suggests an antenna operating in the Ku frequency band at two bands spanning 12.47–13.08 GHz and 16.51–17.42 GHz. The frequency bands of the CP are 12.39–13.56 GHz and 16.3–17.65 GHz. This antenna is designed for satellite applications. Besides in [21], the proposed fractal antenna is fabricated on an FR4 substrate ($\varepsilon_r = 4.4$), providing an overall size of 36.6 mm $\times$ 36.6 mm $\times$ 1.6 mm. This antenna offers CP in the frequency band from 17.12 to 18.04 GHz and operates within the band of 16.96–18.74 GHz, presenting a maximum gain of 5.14 dBi. All these antennas provide a narrow operating BW alongside limited CP BW.

In contrast to the antenna designs, as cited in the above references, which are developed based on parametric analysis, this study combines the truncation of two opposite corners of the square patch antenna to create CP and the powerful genetic algorithm extension named MOGA, automating the process to enhance antenna performance. This integration helps overcome the limitations of the operating and axial-ratio bandwidths. This antenna is developed to operate within the 13.2-–15.1 GHz frequency band to cover satellite communication applications [22], including aeronautical mobile, aviation, radio astronomy, and Industrial, Scientific, and Medical (ISM) systems. The optimized CP antenna is printed on an FR4 epoxy substrate ($\varepsilon_r = 4.4$) due to its high mechanical rigidity and low cost, providing a compact structure with an overall size of $20 \times 20 \times 1.6\,\text{mm}^3$. Moreover, it operates within a wide frequency band spanning from 12,18 GHz to 15,85 GHz. The broadened 3-dB ARBW covers the frequency band from 12.92 GHz to 15.29 GHz, offering CP across this band.

The organization of the remaining sections is as follows. Section 2 presents the geometry of the suggested CP antenna, general steps of the MOGA, the developed MOGA, and different steps involved in optimizing the antenna performance. Section 3 displays the frequency response, far-field results, corresponding equivalent circuit of the CP antenna, and the comparative analysis of the optimized antenna performance with relevant published studies. The last section presents a summary of the key results discussed in this paper.

2. STRUCTURE AND CP ANTENNA PARAMETERS

2.1. Geometry and Parameters of the Proposed Antenna

The suggested antenna design is presented in Fig. 1. As indicated in this figure, the patch antenna is etched on the front side, while the ground plane is etched on the back side. The trimmed-corner square patch antenna with dimensions of $R_1 + C_1$ is exited using a feedline with the length of $L_1 + L_2 + L_6$. This antenna shape is used to generate the CP. To broaden the obtained frequency band of CP, four square parasitic elements are added on front side of the antenna, and a rectangular slot is introduced in the center of the square patch. Also, a rectangular slot is cut in the ground plane under the feedline to expand the operating frequency band. The ground plane and patch antenna are printed on an FR4 substrate ($\varepsilon_r = 4.4$). The overall size of the antenna is 20 mm $\times$ 20 mm $\times$ 1.6 mm. The parameter values in Table 1 are the optimized dimensions applying MOGA.

TABLE 1. Parameters and their associated values of the optimized CP antenna.

Parameters	values (mm)	Parameters	values (mm)
W	20	f_1	3
L	20	f_2	0.6
H	1.6	f_3	1
P_1	2.5	f_4	2
P_2	3	L_1	1
P_3	4	L_2	2.8
P_4	0.5	L_3	2
R_1	6.8	L_4	1.4
C_1	3.2	L_5	1
L_6	0.7		

2.2. Multi-Objective Genetic Algorithm Steps

Based on the process of natural selection derived from biological evolution, genetic algorithms (GAs) are potent optimization

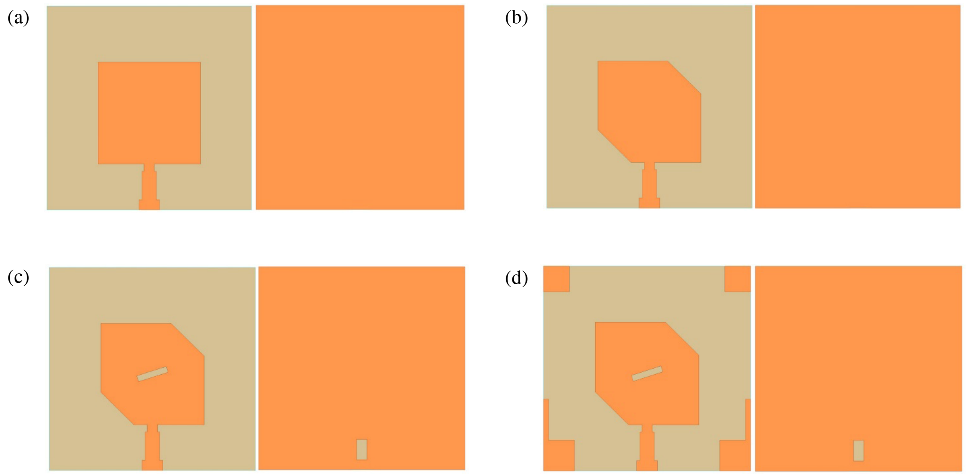

FIGURE 2. Parametric evolution of the proposed circularly polarized antenna: (a) initial design, (b) corner-truncated path, (c) addition of the diagonal slot and ground modification, and (d) final optimized antenna configuration.

TABLE 2. MOGA parameters during the optimization procedure.

MOGA parameters and operators	Attribute Descriptions
Iteration numbers	180
time	36 h 21 min
selection operator	selectiontournament
crossover function	crossoverscattered
mutation function	mutationpower

techniques. They simulate how populations of organisms develop over many generations, adjusting to their environment to survive and procreate efficiently. When used to solve problems, GAs evolve a population of candidate solutions instead of a single solution. An extension of genetic algorithms called MOGA is developed for problems with multiple objectives. Several steps are involved to achieve the desired objectives, and the general ones can be described as follows. The parametric study of the proposed circularly polarized (CP) antenna is presented in Fig. 2, while the results of the multi-objective genetic algorithm (MOGA) optimization are summarized in Table 2. In the first step, a random population is generated within the lower and upper parameter bounds, including different chromosomes (individuals). Then, in the second step, the parent population is evaluated by calculating the values for all objective functions based on the issue formulation for each parent chromosome. These objective values measure the performance of each chromosome with respect to the defined objective functions. If the conditions were satisfied, the procedure was stopped; otherwise, in the third step, a new population called child population was generated using different techniques comprising selection, crossover, and mutation functions. The selection function is applied on the parent population to choose individuals for the next generation. Numerous methods can be used, and one of them is the Selection Wheel Roulette [23]. This operator selects parents by simulating a roulette wheel, in which the area of the wheel section corresponding to an individual is proportional to its fitness value. The algorithm uses a random number to select one of the sections with a probability equal to its area. Moreover, tournament selection [23] may be employed. This operator randomly picks a certain number n of people from the whole group to compete against each other. The tournament winner is the individual with the greatest fitness value. This individual is then chosen for further processing in the genetic algorithm, which includes crossover and mutation. This method is repeated to pick the required number of parents for the following generation. This selection approach balances the promotion of fitter individuals while retaining genetic variety through random sampling. In the next step, the crossover function is used to create the next population (child population). Several approaches exist, among which the crossover scattered operator (random mask crossover) [24, 25] produces the child population by creating a random binary vector (mask) with the same parent chromosome size, retaining variety while exploring novel solution combinations. For each component point, if the mask value is 1, the child's gene is picked from parent 1; otherwise, the gene is taken from parent 2. Furthermore, single-point crossover develops new individuals by joining two parent solutions [24, 26, 27]. Here is how it works: Initially, two parent chromosomes are picked. Then, a random crossover position along the chromosomal length is determined. The children are generated by exchanging the segments of the parents after this crossing point. This means that one child receives the genes from the first parent up to the crossover point and the remaining genes from the second parent, while the other child receives the complementary portions. Besides, two-point crossover selects two distinct random points along the chromosome length and swaps the middle segment between the two parent solutions to create offspring [24, 26]. Specifically, for parents P_1 and P_2, randomly choose the crossover points i and j ($1 \leq i < j \leq L$, where L is chromosome length); $child_1$ receives genes 1 to $i-1$ from P_1, i to j from P_2, and $j+1$ to L from P_1; $child_2$ receives the complementary segments. Additionally, Laplace crossover is a parent centric operator [28, 29], and this function uses two parent individuals P_1 and P_2 to generate the children individuals $child_1$ and $child_2$ based on Laplace distribution using Eq. (1). First, two random numbers k_i and k_i^j are generated using the uniform distribution between 0 and 1. Then, a random number α_i is generated using the Laplace distribution as indicated in Eq. (1).

$$\alpha_i = \begin{cases} a - b\log(k_i), & k_i^j \leq 0.5 \\ a + b\log(k_i) & k_i^j > 0.5 \end{cases} \tag{1}$$

where a is the location parameter, and the scale parameter $b > 0$. The parameter b controls how the children are distributed around the parents. The scale parameter is set to $b = b_{real}$ for real-valued variables and to $b = b_{int}$ for decision variables that are limited to integers. This distinction is crucial because the nature of the variables should be reflected in the perturbation scale. While smaller values of b encourage producing children farther from the parents, supporting broader exploration of the search space, smaller values of b cause offspring to be generated closer to their parent solutions, encouraging local search. The two children $child_1$ and $child_2$ are obtained as follows:

$$child_1 = P_1 + \alpha_i |P_1 - P_2| \tag{2}$$

$$child_2 = P_2 + \alpha_i |P_1 - P_2| \tag{3}$$

After the crossover process combines the parent individuals to generate new children, mutation is applied to introduce random variations into these offspring. This step guarantees genetic diversity, allowing the algorithm to explore new regions of the solution space and avoid premature convergence. Numerous mutation operators can be used, including Gaussian Mutation, Adaptive Directed Mutation, and Power Mutation. The Gaussian Mutation technique requires two crucial parameters: the mean and the standard deviation [29]. Typically, to demonstrate that mutations are centered around the current gene value, the mean is set to zero, guaranteeing no systematic bias in the mutation direction. Where σ is the standard deviation, it controls the mutation strength by defining the spread of the distribution; a larger σ leads to more significant variations in the mutated gene, while a smaller σ results in subtle changes. Mathematically, the Gaussian distribution used for mutation is given by the following equation:

$$f(x) = \frac{1}{\sqrt{2\pi\sigma^2}} \exp\left(-\frac{(x-\mu)^2}{2\sigma^2}\right) \tag{4}$$

where μ is the mean (usually zero), and x represents the mutation value added to the gene. This formula describes the probability density function of the Gaussian distribution, guiding how mutation values are sampled to perturb genes during the evolutionary process. Moreover, the Adaptive Directed Mutation operator is designed to prevent gene concentration caused by crossover and to avoid random [30]. It generates new solutions guided by an adaptive gradient direction based on previous solutions, which informs the search process. This gradient direction is derived from changes in fitness values of the individuals over three consecutive generations, capturing how each solution evolves during optimization, while Power Mutation mutates the parent y, utilizing equation (5) [29]. For each element of the parent population, the jth component of the child x is given as follows:

$$x(j) = \begin{cases} y(j) - s(y(j) - lb(j)) & \text{if} \quad t(j) < r(j) \\ y(j) + s(ub(j) - y(j)) & \text{if} \quad t(j) \geq r(j) \end{cases} \tag{5}$$

Here, $t(j)$ is the distance of $x(j)$ from the jth component of the lower bound $lb(i)$ and is mathematically calculated using Eq. (6); r is a random number calculated from a uniform distribution in the unit interval; s is a random variable, which is generated according to the power distribution using Eq. (7), where p is a random created number between 0 and 1.

$$t(j) = \frac{y(j) - lb(j)}{ub(j) - lb(j)} \tag{6}$$

$$f(k) = pk^{p-1} 0 \leq k \leq 1 \tag{7}$$

The fourth step of the optimization process is dedicated to scoring the children. If the stopping condition (Maximum number of generations, MaxStallGenerations, time limit, obtain the targeted one) objectives are achieved, terminate and return the current population; otherwise, proceed to the next step, where the parent population and the children are combined into an extended population [31]. Then, the individuals of the obtained population were sorted by computing the rank and crowding distance using the subsequent steps:

a) Compute the rank using the fast non-dominated sorting algorithm, identify the non-dominated fronts F_1, F_2, …, F_k in the extended population. Repeat step b for each front $i = 1, \ldots, k$ [31].

b) Calculate the crowding distance for each individual in F_i as demonstrated in Eq. (8) [31]. In ascending order, sort the solutions in F_i for each objective function r. Let m be the number of individuals in F_i, and $y_{[j,r]}$ represents the *j-th* solution in the ranked list with respect to the objective function r. Assign $cd_r(y_{[1,r]}) = \infty$ and $cd_r(y_{[m,r]}) = \infty$, and for $j = 2, \ldots, m-1$, assign the crowding distance value according to Eq. (8). To obtain the total crowding distance *cd(y)* of a solution y, sum the solution's crowding distances for all objective functions (Eq. (9)).

$$cd_r\left(y_{[j,r]}\right) = \frac{Z_r\left(y_{[j+1,r]}\right) - Z_r\left(y_{[j-1,r]}\right)}{Z_{r;Max} - Z_{r,Min}} \tag{8}$$

$$cd(y) = \sum_r cd_r(y). \tag{9}$$

In the last step, the extended population is trimmed to obtain the population size of individuals by retaining the desired number of individuals of each rank. Apply the crossover and mutation operators to the selected population and go to step 4 [31].

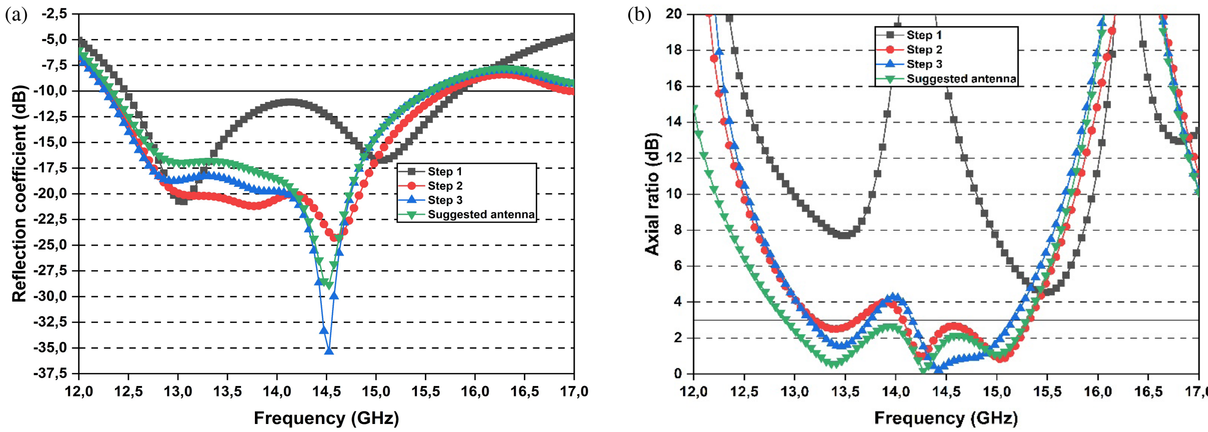

FIGURE 3. Evolution of the proposed circularly polarized antenna design: (a) reflection coefficient (S_{11}) and (b) axial ratio (AR) of Step 1, Step 2, Step 3, and the proposed antenna.

3. DIFFERENT CP ANTENNA STEPS

To gain a comprehensive understanding of the proposed antenna approach to generate CP, Fig. 3 depicts the procedure to build the antenna structure from a basic square patch to a trimmed-corner patch antenna with parasitic elements. The obtained reflection coefficient and axial ratio are illustrated in Fig. 3.

In the first step (Fig. 2(a)), the antenna is designed based on a conventional square patch to operate within the desired frequency band. The obtained reflection coefficient indicates that the antenna functions within the target band; however, improved impedance matching is still required. Additionally, the axial ratio exceeds 3 dB, indicating that the antenna does not exhibit circular polarization. In the second step (Fig. 2(b)), two opposite corners of the square patch are truncated to generate circular polarization. As shown in Fig. 3(a), the antenna achieves circular polarization in dual bands, from 13.3 to 13.4 GHz and from 14.2 to 15.4 GHz, while the reflection coefficient bandwidth spans from 12.4 to 15.6 GHz. In the third step (Fig. 2(c)), two slots are etched at the center of the truncated patch and beneath the feeding line to enhance the axial ratio bandwidth. As illustrated in Fig. 3(a) and Fig. 3(b), the antenna achieves circular polarization over a wider band ranging from 12.4 to 15.6 GHz. In the final step (Fig. 2(d)), four square and two rectangular parasitic elements are introduced on the front side to modify the current distribution, thereby broadening the axial ratio bandwidth. The corresponding reflection coefficient and axial ratio, based on the optimized antenna dimensions, demonstrate that the impedance bandwidth ranges from 12.34 to 15.55 GHz, while the 3 dB axial ratio bandwidth extends from 12.92 to 15.29 GHz.

4. DEVELOPED MULTI-OBJECTIVE GENETIC ALGORITHM

The multi-objective genetic algorithm (MOGA), implemented using MATLAB and ANSYS Electronics Desktop, is employed to optimize the reflection coefficient bandwidth (RCBW) and axial ratio bandwidth (ARBW). The optimization process is fully automated using IronPython.

In this section, the procedure for implementing the MOGA script using MATLAB's Global Optimization Toolbox is described. The optimization is performed using the function *gamultiobj (fun, nvars, A, b, Aeq, beq, lb, ub, options)*, where *fun* represents the fitness function to be optimized; *nvars* denotes the number of variables; A and b define the linear inequality constraints; *Aeq* and *beq* represent the linear equality constraints; *lb* and *ub* correspond to the lower and upper bounds of the variables, respectively; and *options* specify the optimization settings.

The outputs of this function include *(x, fval, exitflag, output, population, scores)*, where ***x*** represents the Pareto-optimal solutions; *fval* contains the corresponding objective function values on the Pareto front; *exitflag* indicates the termination condition of the algorithm; *output* provides information about the optimization process; *population* denotes the final population; and *scores* represent the fitness values of the final population.

To optimize the reflection coefficient and axial ratio of the proposed antenna, the Fitness functions F_S and F_{AR} are defined as demonstrated in Eqs. (10) and (11) to minimize the reflection coefficient and axial ratio to be < -10 dB and < 3 dB, respectively, in the band from 13.2 GHz to 15.1 GHz.

$$F_S = \max(|S_{11}(f_i)|) \quad (10)$$

$$F_{AR} = \max(AR(f_i)) \quad (11)$$

where $f_i \in [13.2\ 15.1]$.

The most critical variables that influence RCBW and ARBW are described by the following vector $[C_1\ R_1\ f_1\ f_2\ P_1\ P_2\ P_3\ P_4]$, and the lower bound is given by [2 4 1 0.2 1.5 2 3 0.2], while the upper bound is [4 8 4 1.5 3.5 4.5 6 1]. The chosen optimization options for this study are as follows. The chosen selection function is 'selectiontournament', and the maximum generations and population size are set to 10 and 40, respectively. To explore the parameter space, 'crossoverscattered' is used. To gain more diversity, the mutation function 'mutationpower' is utilized. The flowchart of the optimization process is illustrated in Fig. 4. In the first

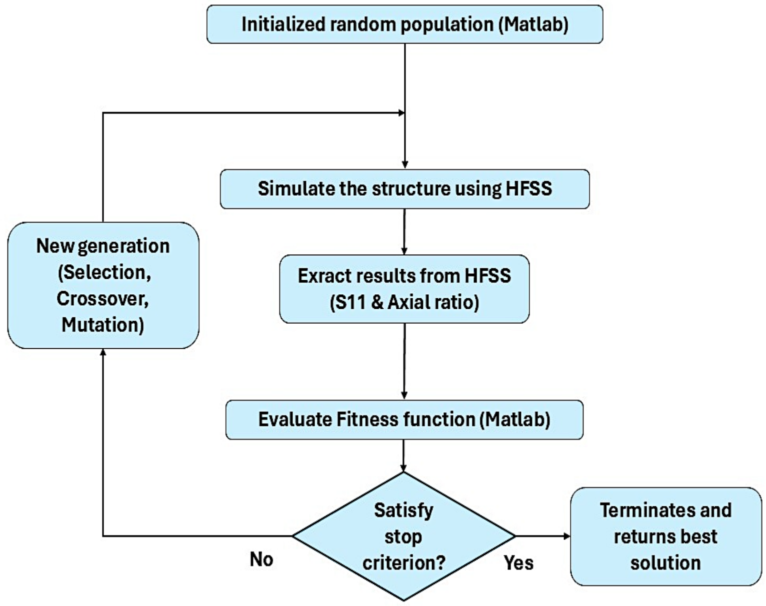

FIGURE 4. Flowchart of the optimization process.

step, an initial population is generated randomly considering the lower and upper bounds. This population is named as the parent population; it comprises 40 individuals. In the next step, for each individual, the antenna structure is simulated using High Frequency Structure Simulator (HFSS). Then, the obtained reflection coefficient and axial ratio values are extracted in a CSV file and uploaded to MATLAB to evaluate the fitness functions. If the stop criterion is satisfied, the process terminates and returns the best solution; otherwise, a new population called the child population is generated using the parent population. First, the parent population is selected using 'selectiontournament' with a tournament size of 3, and a random subset of individuals is selected. During the tournament, each individual is evaluated, and then the individual with the highest fitness score is added to the selection pool. This process was repeated to obtain the desired number of individuals for the next generation. Second, to explore the parameter space effectively, the crossover function is implemented using 'crossoverscattered'. To survey more diversity within the population, the 'mutationpower' function is implemented. The structure was simulated again using the children's population. This process will be repeated until one of the stopping conditions is satisfied. For this optimization, the maximum generations is set to 300; MaxStallGenerations is configured as 100; and Function Tolerance is set to 10^{-4}.

5. OBTAINED RESULTS OF THE OPTIMIZED CP ANTENNA

5.1. Frequency Response and Farfield Results of the Proposed Optimized Antenna with MOGA

The optimal antenna performance is achieved by employing the robust MOGA, which effectively balances conflicting objectives including reflection coefficient and axial ratio to find a set of Pareto-optimal solutions. This algorithm allows for simultaneous optimization of several parameters, ensuring strong exploration of the solution space. It helps obtain the desired goals in the suitable frequency range from 13.2 GHz to 15.1 GHz, including good matching of the antenna impedance to be less than -10 dB and to ensure the CP indicated by the observed 3 dB ARBW. After applying the optimization process, the optimal parameter values for C_1, R_1, f_1, f_2, P_1, P_2, P_3, and P_4 are obtained as 3.2 mm, 6.8 mm, 3 mm, 0.6 mm, 2.5 mm, 3 mm, 4 mm, and 0.5 mm, respectively.

Figure 5 shows simulated results using HFSS and Computer Simulation Technology (CST) software for validation, comprising the reflection coefficient, voltage standing wave ratio (VSWR), axial ratio, peak gain, radiation efficiency, and input impedance. To confirm the simulated results, the epoxy FR4 substrate was used to produce a prototype of the antenna, as indicated in Fig. 6(a) and Fig. 6(b). Then, the reflection coefficient and VSWR were measured using the 3656D Vector Network Analyzer (VNA) (Fig. 6(c)). The proposed antenna provides a broad operating frequency band achieved utilizing HFSS spans from 12.35 GHz to 15.53 GHz, while that obtained with CST ranges from 12.37 GHz to 15.7 GHz; however, the measured bandwidth is from 12,18 GHz to 15,85 GHz, thus validating the simulated results. The impedance matching is confirmed by plotting the VSWR, as depicted in Fig. 5(b), the simulated and measured VSWRs are below 2 in the operating frequency band, validating good impedance matching. To evaluate the polarization behavior of the antenna, the axial ratio is assessed as a key parameter across the desired frequency range. Fig. 5(c) shows that the simulated axial ratio using HFSS and CST is below 3 dB in the wide frequency band from 12.92 GHz to 15.29 GHz. Also, the suggested CP antenna provides an important gain, achieving a maximum gain of 5.9 dBi. Moreover, Fig. 5(e) shows radiation efficiency, reaching a maximum of 77.77%.

The discrepancies between the results obtained using HFSS and CST software mainly stem from their distinct numerical techniques and meshing strategies. HFSS utilizes the Finite

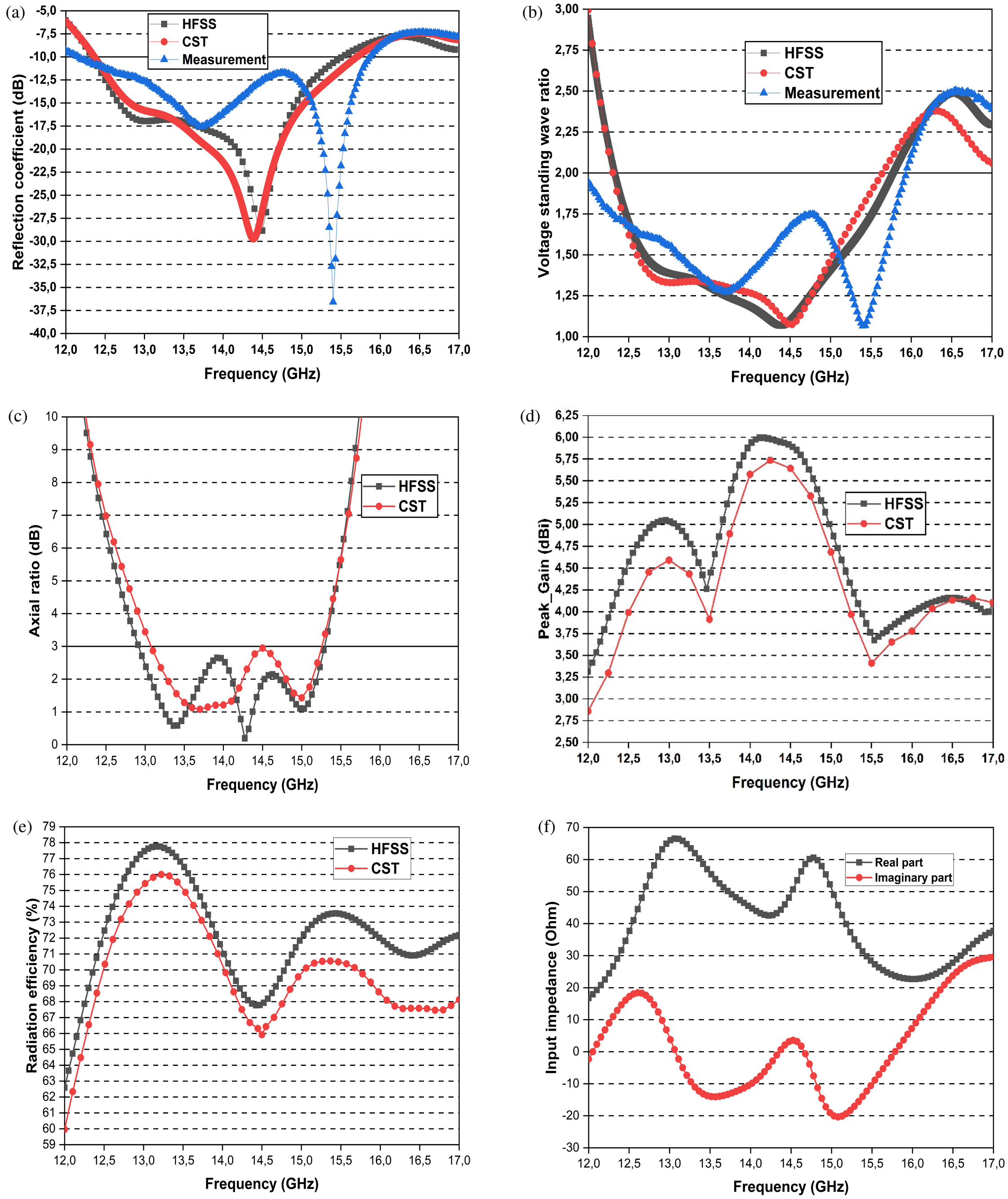

FIGURE 5. Achieved results: (a) reflection coefficient, (b) VSWR, (c) axial ratio, (d) peak gain, (e) radiation efficiency, and (f) input impedance.

Element Method (FEM), whereas CST primarily uses the Finite Integration Technique (FIT), and the observed difference between the measured and simulated reflection coefficients is due to the soldering effect, SMA connector, measurement uncertainty, environmental effects, and fabrication imperfections.

Figure 7 presents the surface current distribution of the optimized CP antenna at the resonant frequency of 14.47 GHz. The surface current rotates in a clockwise direction, indicating that the suggested antenna generates right-hand circular polarization (RHCP).

To evaluate the radiation patterns in different planes, as seen in Fig. 8(a) and Fig. 8(b), the far-field radiation patterns are plotted in E and H planes at an operating frequency of 14.47 GHz, respectively. In both planes, the suggested antenna pattern is unidirectional. In addition, the 3D radiation pattern shows how an antenna directs its energy. As demonstrated in Fig. 8(c), the suggested CP antenna provides strong radiation performance, achieving a remarkable gain of 5.9 dBi at 14.47 GHz.

6. EQUIVALENT CIRCUIT

The equivalent circuit model is used to achieve a deeper understanding of antenna performance, providing a reduced yet pow-

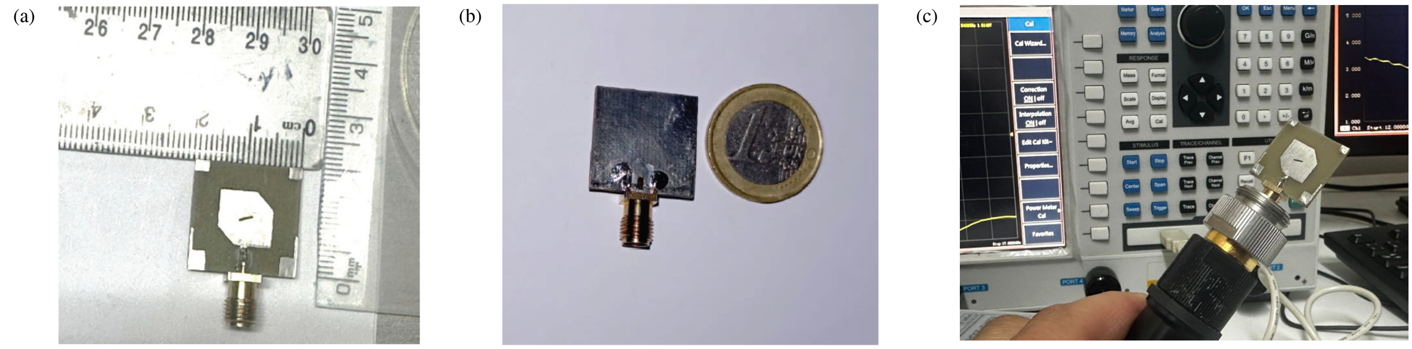

FIGURE 6. Fabricated prototype of the proposed design, (a) front view, (b) back view, and (c) measurement configuration using a calibrated vector network analyzer.

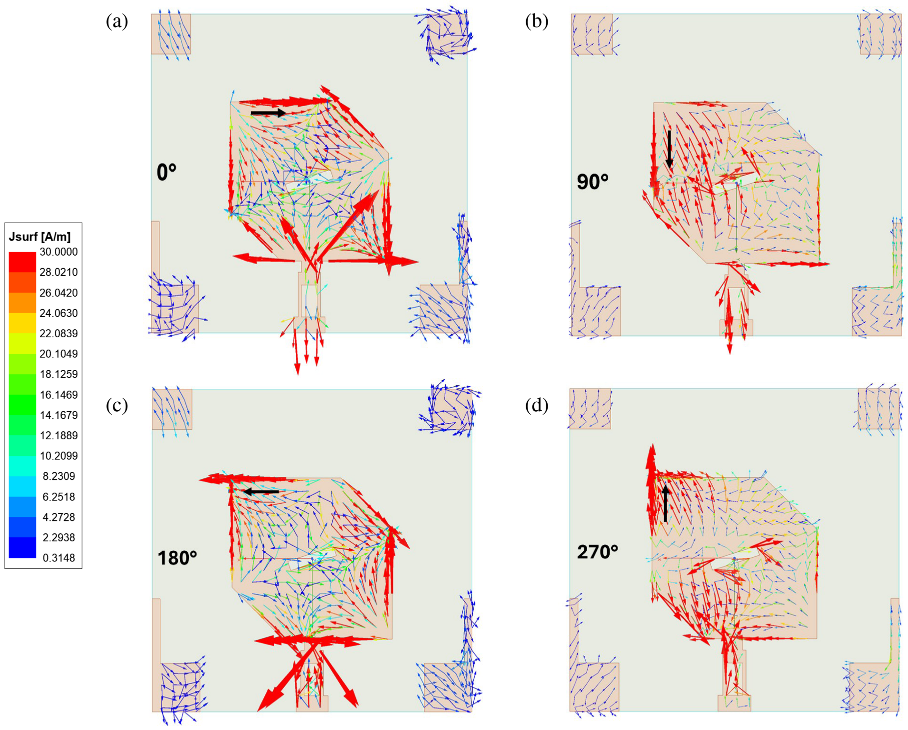

FIGURE 7. Distribution of the surface current vector on the top surface analyzed at multiple phase angles: (a) 0°, (b) 90°, (c) 180°, (d) 270°.

erful representation of antenna electrical characteristics. For the suggested CP antenna, the electrical equivalent network model is designed with the Advanced Design System (ADS) by integrating multiple resonators arranged sequentially.

As indicated in Fig. 9(a), the antenna electrical behavior is modeled by two parallel $R_1L_1C_1$ and $R_2L_2C_2$ elements based on the input impedance maxima, as demonstrated in Fig. 5(f). The real part of the input impedance exhibits two distinct maxima, and each is presented with parallel RLC elements, whereas C_0 is connected in series with the inductance L_0, presenting the capacitance and inductance of the antenna feedline. On the other hand, the parasitic patches are represented with their capacitances C (C_3, C_4, C_5, and C_6) and inductances L (L_3, L_4, L_5, and L_6). Moreover, the central patch is linked with parasitic patches via coupling capacitances C_m (C_{m1}, C_{m2}, C_{m3}, and C_{m4}). The optimal values of L_0, C_0, R_1, L_1, C_1, R_2, L_2, and C_2 are achieved utilizing the powerful ADS's optimization. Consequently, the optimal values of L_0, C_0, R_1, L_1, C_1, R_2, L_2, C_2, L_3, C_3, L_4, C_4, L_5, C_5, L_6, C_6, C_{m1}, C_{m2}, C_{m3}, and C_{m4} are depicted in Table 3. As illustrated in Fig. 9(b), the equivalent circuit bandwidth ranges from 12.45 GHz to 15.7 GHz, guaranteeing good agreement with the measured and the simulated results.

7. COMPARISON OF THE ACHIEVED RESULTS WITH RELEVANT PUBLISHED STUDIES

The performance examination of the proposed CP antenna is displayed in Table 4, comprising the overall size, ARBW, RCBW, radiation efficiency, and maximum gain. This table demonstrates that the optimized antenna provides the operating frequency band 12.18–15.85 GHz, wider than the bandwidths in [21, 32, 33, 34]. Also, the CP bandwidth ranges from 12.92 to 15.29 GHz, larger than all presented references in this table.

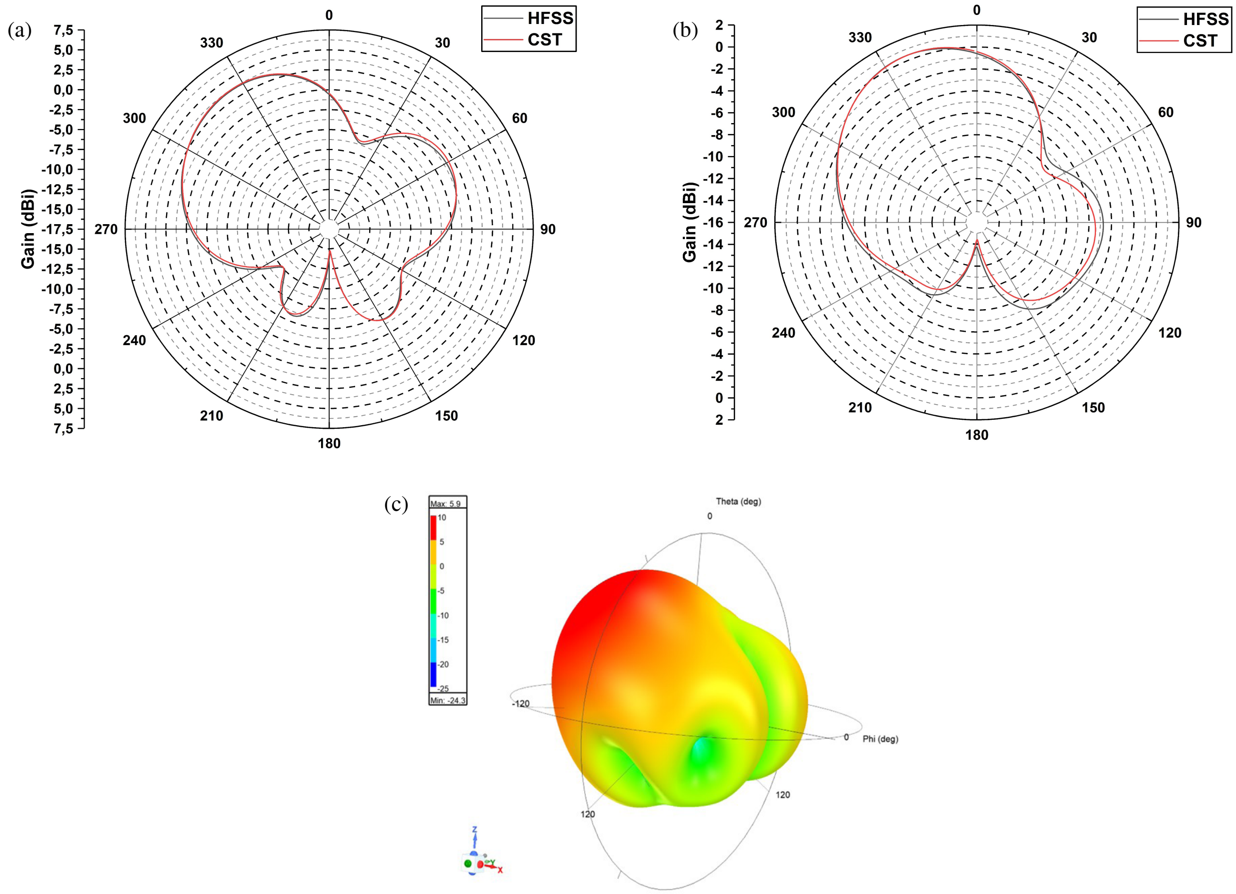

FIGURE 8. Proposed antenna radiation pattern characteristics, (a) E plane, (b) H plane, (c) 3D radiation pattern at 14.47 GHz.

TABLE 3. The equivalent circuit components and their corresponding values.

Components of the equivalent circuit and the corresponding values			
$R_1 = 46.3221$ Ohm	$L_3 = 32.0013$ nH	$C_1 = 573.312$ fF	$C_6 = 446.536$ fF
$R_2 = 63.4367$ Ohm	$L_4 = 639.897$ fH	$C_2 = 510.376$ fF	$C_{m1} = 992.707$ fF
$L_0 = 1.99439$ nH	$L_5 = 1.71548$ nH	$C_3 = 2.05959$ pF	$C_{m2} = 1.17694$ pF
$L_1 = 257.976$ pH	$L_6 = 17.6657$ pH	$C_4 = 3.33249$ pF	$C_{m3} = 154.247$ fF
$L_2 = 788.606$ pH	$C_0 = 89.1382$ fF	$C_5 = 881.726$ fF	$C_{m4} = 26.549$ fF

TABLE 4. Analysis and comparison of the optimized CP antenna performance with the prior research.

Ref	**Entire dimensions (mm^3)**	**ARBW (%)**	**RCBW (%)**	**Efficiency (%)**	**Max gain (dBi)**
[33]	$96.435 \times 50.017 \times 1.64$	0	2.87	NM	7.627
[20]	$72 \times 72 \times 14.388$	9.15/7.97	4.8/5.37	NM	14.91
[21]	$36.6 \times 36.6 \times 1.6$	5.21	10.01	86	5.14
[32]	$40 \times 48 \times 1.59$	2.56/3.57	6.27/7.60	NM	8.01–6.01
Optimized antenna	$20 \times 20 \times 1.6$	16.68	26,14	67	5.9

Moreover, the overall size of the optimized antenna is more compact than antennas in [19, 20, 21, 32]. The achieved gain of the CP antenna, close to 5.9 dBi, is achieved at the frequency value of 14.17 GHz, presenting a reasonable gain. Furthermore, the radiation efficiency exceeds 67%. These results confirm the antenna's adequacy for satellite applications requiring reliable signal transmission and reception within the operating bandwidth.

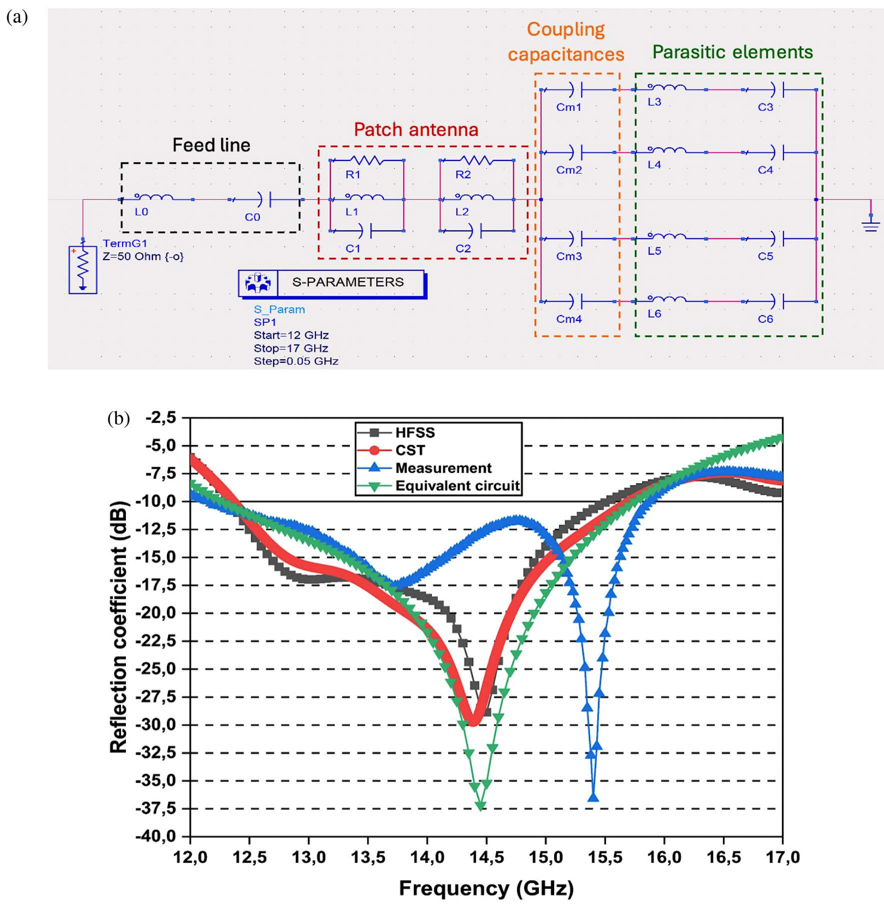

FIGURE 9. Electrical behavior of the optimized antenna, (a) equivalent circuit and (b) the reflection coefficient comparison obtained with HFSS, CST, measurement, and ADS.

8. CONCLUSION

In this study, the proposed circularly polarized (CP) antenna is designed and fabricated on an FR-4 epoxy substrate with a compact size of 20 mm × 20 mm × 1.6 mm, featuring a simple single-layer structure. The antenna is developed for Ku-band applications using a multi-objective genetic algorithm (MOGA), achieving high performance in terms of a wide operating bandwidth, broad axial ratio bandwidth (ARBW), reasonable gain, and good radiation efficiency. The reflection coefficient bandwidth (RCBW) ranges from 12.18 GHz to 15.85 GHz. Moreover, the antenna exhibits circular polarization within the frequency range of 12.92 GHz to 15.29 GHz, supporting RHCP and ensuring robust signal quality. It achieves a peak gain of 5.9 dBi and a radiation efficiency of up to 67% across the operating band. These characteristics make the proposed CP antenna well-suited for mobile applications in the Ku frequency band.

ACKNOWLEDGEMENT

The authors would like to express their sincere gratitude to Universiti Teknikal Malaysia Melaka (UTeM) and the Ministry of Higher Education (MoHE), Malaysia, for providing the necessary facilities, resources, and support for this research. Additionally, the authors gratefully acknowledge Asia Pacific University (APU) and the Strategic Research Institute (SRI) for their continuous support.

REFERENCES

[1] Sharma, S., A. Kumar, R. Kumar, N. K. Saluja, Z. Zakaria, and A. J. A. Al-Gburi, "Miniaturized ultrawideband circularly polarized antenna with enhanced axial ratio bandwidth for C-band automotive and satellite applications," *Progress In Electromagnetics Research C*, Vol. 161, 159–168, 2025.

[2] Yadav, S. K., A. Gupta, V. Kumar, D. K. Garg, and A. J. A. Al-Gburi, "Prediction of axial ratio using machine learning (ML) for a dual-band circularly polarized dielectric resonator antenna (DRA)," *Chinese Journal of Physics*, Vol. 96, 1364–1384, 2025.

[3] Bennioui, F.-Z., A. Khabba, K. A. Bouslam, L. Wakrim, S. Ibnyaich, A. Zeroual, Z. Zakaria, and A. J. A. Al-Gburi, "Genetic algorithm optimization of a wideband rectangular patch antenna with an asymmetric u-slot and partial ground for ku-band satellite communication," *Progress In Electromagnetics Research M*, Vol. 133, 51–60, 2025.

[4] Azzouz, A., R. Bouhmidi, M. Chetioui, R. Berber, and A. J. A. Al-Gburi, "Design and performance analysis of a fan-shaped fractal antenna for radar systems and satellite communications," *Journal of Optoelectronics and Advanced Materials*, Vol. 28, No. 1-2, 20–30, 2026.

[5] Al-Gburi, A. J. A., I. B. M. Ibrahim, Z. Zakaria, and N. F. B. M. Nazli, "Wideband microstrip patch antenna for sub 6 GHz and

5G applications," *Przegląd Elektrotechniczny*, Vol. 11, 26–29, 2021.

[6] Shrivastava, M. K., R. Singh, D. Samantaray, A. Khan, A. K. Gautam, and A. K. Singh, "A metamaterial loaded high gain low profile RHCP microstrip antenna for X-band applications," *IEEE Access*, Vol. 13, 33 321–33 329, 2025.

[7] Nguyen-Huy, H., D.-N. Tran-Viet, P. Kim-Thi, and H. Tran-Huy, "Compact high-gain circularly polarized patch antenna based on TM30/TM03 mode," *PLoS One*, Vol. 20, No. 5, e0321091, 2025.

[8] Hossain, A. R., M. S. I. Sagar, A. A. Mertvyy, P. K. Sekhar, and T. Karacolak, "Inkjet printed flexible dual-band dual-sense circularly polarized patch antenna," *IEEE Access*, Vol. 12, 55 424–55 433, 2024.

[9] Arora, C. and S. S. Pattnaik, "Particle swarm optimization based metamaterial inspired circularly polarized patch antenna for s band applications," *Evolutionary Intelligence*, Vol. 14, No. 2, 801–810, 2021.

[10] Thommandru, R. and R. s. kumar, "Cost-effective circularly polarized MIMO antenna for Wi-Fi applications," *Indonesian Journal of Electrical Engineering and Computer Science (IJEECS)*, Vol. 36, No. 2, 2024.

[11] Fayyaz, U., S. A. Niazi, K. Al-Jaloud, W. A. Malik, A. Aziz, R. Hussain, A. H. Alqahtani, and A. Alomainy, "Design of a microstrip line fed SIW ring antenna with sixth-order circular polarized conical pattern," *IEEE Access*, Vol. 13, 135 466–135 474, 2025.

[12] Ait Lahcen, A., S. Chabaa, S. Ibnyaich, and A. Zeroual, "An enhanced octagonal microstrip patch antenna circularly polarized for WIMAX and 5G mid-band applications," in *2024 International Microwave and Antenna Symposium (IMAS)*, 1–5, Marrakech, Morocco, 2024.

[13] Elabd, R. H. and A. J. A. Al-Gburi, "Design and optimization of a circular ring-shaped UWB fractal antenna for wireless multiband applications using particle swarm optimization," *Progress In Electromagnetics Research B*, Vol. 106, 101–112, 2024.

[14] Bahlaouane, I., A. Belhabib, S. Ibnyaich, and A. Zeroual, "Optimization and performance enhancement of a miniaturized rectangular patch antenna with slotted ground plane using ant colony algorithm," in *ITM Web of Conferences*, Vol. 69, 04011, 2024.

[15] Ma, Z. and J. Liu, "An improved NSGA-II algorithm for multiobjective optimization of irregular polygon patch antennas," *Micromachines*, Vol. 16, No. 7, 786, 2025.

[16] Sellak, L., A. Khabba, S. Chabaa, S. Ibnyaich, A. Baddou, A. Zeroual, and T. Sutikno, "ANN-based design of miniaturized circular dual-band 4 × 4 MIMO antenna for 28/38 GHz 5G mmWave applications," *TELKOMNIKA (Telecommunication Computing Electronics and Control)*, Vol. 22, No. 5, 1280–1292, 2024.

[17] Sellak, L., A. Khabba, S. Chabaa, S. Ibnyaich, V. K. L. Yong, A. Baddou, and A. Zeroual, "RBFNN-based UWB 4 × 4 MIMO antenna design with compact size, high isolation, and improved diversity performance for millimeter-wave 5G applications," *Physica Scripta*, Vol. 99, No. 6, 066007, 2024.

[18] Abdelhady, A. M., H. A. Mohamed, W. A. E. Ali, and A. A. Ibrahim, "High gain quad-port circularly polarized aperture-coupled MIMO antenna," *Scientific Reports*, Vol. 15, No. 1, 32606, 2025.

[19] Naik, D. K., D. C. Panda, R. Swain, A. Muduli, and A. Pal, "Characteristic mode inspired broadband circularly polarized metasurface antenna with triple-mode excitation for Sub-6 GHz applications," *Scientific Reports*, Vol. 15, No. 1, 33965, 2025.

[20] Luo, W., X. Wang, X. He, and Y. Yang, "High gain dual-frequency dual-circularly polarized fabry perot resonant cavity antenna for Ku band," *Progress In Electromagnetics Research Letters*, Vol. 125, 1–7, 2025.

[21] Mohanty, P., S. Pandav, and S. K. Behera, "Circularly polarized hybrid fractal antenna for Ku band application," *AEU — International Journal of Electronics and Communications*, Vol. 190, 155641, 2025.

[22] Bennioui, F. Z., A. Khabba, K. A. Bouslam, L. Wakrim, S. Ibnyaich, A. Zeroual, Z. Zakaria, and A. J. A. Al-Gburi, "Genetic algorithm optimization of a wideband rectangular patch antenna with an asymmetric U-Slot and partial ground for Ku-band satellite communication," *Progress In Electromagnetics Research M*, Vol. 133, 51–60, 2025.

[23] Shukla, A., H. M. Pandey, and D. Mehrotra, "Comparative review of selection techniques in genetic algorithm," in *2015 International Conference on Futuristic Trends on Computational Analysis and Knowledge Management (ABLAZE)*, 515–519, Greater Noida, India, 2015.

[24] Hakimi, D., D. O. Oyewola, Y. Yahaya, and G. Bolarin, "Comparative analysis of genetic crossover operators in knapsack problem," *Journal of Applied Sciences and Environmental Management*, Vol. 20, No. 3, 593–596, Nov. 2016.

[25] Matti, M. S. and A. K. Al-Sulaifanie, "Wavelet denoising based on genetic algorithm," in *2018 International Conference on Advanced Science and Engineering (ICOASE)*, 75–80, Duhok, Iraq, 2018.

[26] Affenzeller, M., S. M. Winkler, S. Wagner, and A. Beham, *Genetic Algorithms and Genetic Programming: Modern Concepts and Practical Applications*, Chapman & Hall/CRC, 2009.

[27] Umbarkar, A. J. and P. D. Sheth, "Crossover operators in genetic algorithms: A review," *ICTACT Journal on Soft Computing*, Vol. 6, No. 1, 1083–1092, 2015.

[28] Deep, K., K. P. Singh, M. L. Kansal, and C. Mohan, "A real coded genetic algorithm for solving integer and mixed integer optimization problems," *Applied Mathematics and Computation*, Vol. 212, No. 2, 505–518, Jun. 2009.

[29] Deep, K. and M. Thakur, "A new crossover operator for real coded genetic algorithms," *Applied Mathematics and Computation*, Vol. 188, No. 1, 895–911, May 2007.

[30] Tang, P.-H. and M.-H. Tseng, "Adaptive directed mutation for real-coded genetic algorithms," *Applied Soft Computing*, Vol. 13, No. 1, 600–614, Jan. 2013.

[31] Konak, A., D. W. Coit, and A. E. Smith, "Multi-objective optimization using genetic algorithms: A tutorial," *Reliability Engineering & System Safety*, Vol. 91, No. 9, 992–1007, 2006.

[32] Naik, K. K. and P. A. V. Sri, "Design of hexadecagon circular patch antenna with DGS at Ku band for satellite communications," *Progress In Electromagnetics Research M*, Vol. 63, 163–173, 2018.

[33] Yanti, R. J., A. I. Wahdiyat, E. T. Rahardjo, F. Y. Zulkifli, and C. Apriono, "Design of a circular patch sub-array microstrip antenna with dual linear polarization for ku-band satellite communication applications," *e-Prime — Advances in Electrical Engineering, Electronics and Energy*, Vol. 11, 100939, 2025.